SHOCK DEVELOPMENT IN AN ELECTROTHERMAL SHOCK TUBE

By B. Campbell,* D. W. George,* and H. K. Messerle*

[*Manuscript received September* 5, 1968]

Summary

The nature of the electrically energized, i.e. electrothermal, shock tube is discussed. It is shown that its performance simulates that of a mechanical shock tube with a hot driver but with a turbulent or unstable driver–shock interface.

I. Introduction

Electrically driven shock tubes produce a fast moving arc tongue, after the energy from a capacitive storage bank has been discharged into a small region at one end of the tube. This arc tongue differs basically from the current-carrying ionizing front in electromagnetically driven tubes since the discharge current producing the tongue is generally extinguished by the time the tongue moves downstream. The arc tongue is analogous to the conventional driver in a mechanical shock tube and a shock region should be expected to form in front of it.

The arc tongue represents a very hot driver and the shock that it can produce must be colder under normal operation. This follows from the need for very high discharge temperatures in order to produce a reasonably high pressure in the discharge region, which may also be called the pressure chamber. If, for example, the temperature in the discharge region is raised at constant mass density from room temperature to 40 000°K in argon, which is initially at a pressure of 5 torr, the pressure will rise at most by a factor of 380. This ratio is of a relatively low order of magnitude when compared with corresponding pressure ratios in mechanical tubes, and the high shock Mach numbers achievable in electrical tubes are due to the high temperatures and associated sound velocities in the discharge chamber and not to the pressure changes.

The existence of a shock region in front of the hot driver has been in doubt for some time. Early papers (Kolb 1959; Sakuntala, Von Engel, and Fowler 1960; George and Messerle 1962; Messerle and George 1963) did not clearly separate these two regions, and it has been found difficult to distinguish experimentally between the very luminous driver and what appeared as a relatively small shock region (Cloupeau 1963; George, Heffernan, and Messerle 1964).

The existence of a colder front was inferred by Cloupeau (1963) from his work on colliding shocks. Kolb (1959) working at Mach numbers in excess of 100 did not distinguish between driver and shock regions. Using electrostatic probes, George, Heffernan, and Messerle (1964) have shown that a low electrical conductivity region exists in front of hot drivers moving at about Mach 10 as long as the experiment is carried out some distance downstream. The shock tube used for this work is shown as Mk. I in Figure 1, and consisted of a fully shielded brass tube with an internal glass liner of 15 mm diameter.

* School of Electrical Engineering, University of Sydney, Sydney, N.S.W. 2006.

In order to investigate this problem more fully a larger capacitor bank was set up and larger diameter and transparent tubes were developed. Various versions of tubes have been used for different purposes, culminating in the very simple Vycor tube assembly shown as Mk. III in Figure 1.

Optical techniques have been used to extend the earlier probe techniques and a streak camera was developed to produce conventional x–t diagrams as well as time-resolved spectra. From these spectral records and measurements of the electrical energy deposited in the driver end, it has been possible to obtain estimates of the temperatures in the different regions of the shock tube. These results together with some high speed framing shots have provided a clear picture of the general shock structure in the electrical shock tubes used.

II. Apparatus

The electrical tubes used consist of a liner divided into the discharge or upstream region and the downstream region by a ring electrode whose surface is flush with the inner wall as shown in Figures 1 and 2. The second electrode is at the upstream end of the tube and the capacitor bank is discharged between these two electrodes. Consequently the high pressure chamber is defined by the region between the ring electrode and the tip of the second electrode.

For optical studies Vycor tubing was found most suitable as liner. The original tubes were fully shielded but this was found unnecessary with the optical equipment since interference from the electrical discharge could be minimized by other means. The protective vacuum glass envelope used earlier (Mk. II in Fig. 1) was also removed to minimize optical distortion. The resulting simple tube structure is shown as Mk. III. The Vycor tubes last much longer than Pyrex tubes before erosion and coating on the inner surface make optical work unreliable. The diameter chosen was 43 mm with 1·5 mm wall thickness.

The electrodes are made of high purity reactor graphite in the case of the central electrode and EG3 for the ring electrode. This material does not seem to have been considered for this application elsewhere (Fowler 1966, for example, preferring platinum), but it has many advantages in a nonreactive atmosphere; it has a high ionization potential and relatively few lines within the visible spectrum. An additional advantage here is its porosity, which we hope to use for gas flow. Both electrodes have graphite liners as working surfaces, these being screwed or pressed into copper for intimate electrical contact.

The electrodes used in earlier tube assemblies were nickel and stainless steel. It was found on using the spectroscope that these materials were seeding the plasma with chromium, nickel, iron, etc. to the extent that argon lines could not be identified because of their weakness. The carbon electrodes improved this situation immediately, so that the resulting spectra consisted of argon II lines together with silicon II and III lines as impurity radiation from the walls.

The system is pumped down through a cold trap using a two-stage backing pump only and flushed several times with argon at atmospheric pressure, and then a continuous purging flow is maintained for the duration of the experiments. The tube pressure ranges from 0·1 to 100 torr and is maintained at the desired value

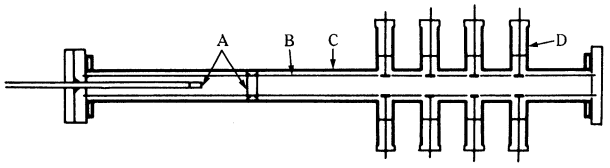

Mk. I

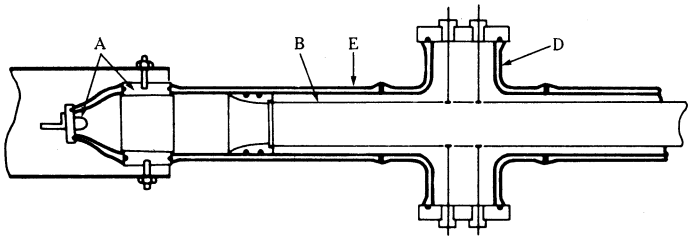

Mk. II

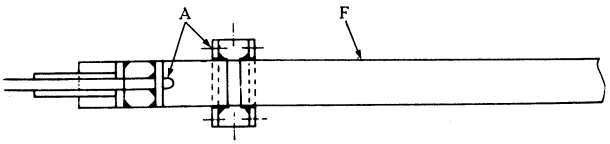

Mk. III

Fig. 1.—Successive stages in the development of the thermally driven electrical shock tubes Mk. I, II, and III: A, electrodes; B, glass liner; C, brass shield; D, probe station; E, Pyrex vacuum envelope; F, Vycor tubing.

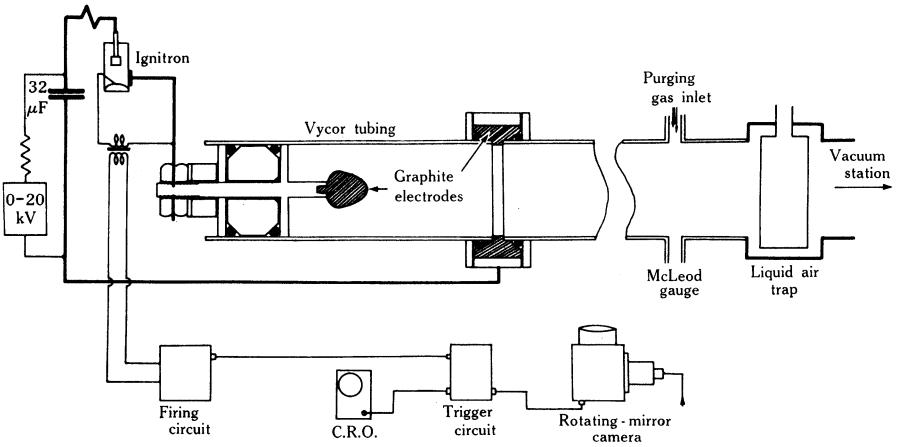

Fig. 2.—Details of the Mk. III shock tube showing ancillary equipment, energy source, and switching and timing circuits.

by adjusting a bleed against the throttled pump. A McLeod gauge is stationed slightly upstream from the purging port. Although the present geometry relies on diffusion upstream to clean the gas there is no evidence in the spectrograms of pump oil contamination (Swan bands) or impurities other than those in the commercially pure argon.

The central electrode is effectively sealed and positioned with internally expanding O-rings and in fact the whole system is held together by O-ring pressure on the Vycor alone; this avoids impurities introduced by adhesive materials.

The electrical circuit (see Fig. 2) consists of a 4 by 8·5 μF 20 kV BICC condenser bank connected to the tube via an ignition. It should be pointed out that the return is not coaxial and that no attempt has been made to employ a magnetic drive by backstrapping etc. The circuit was originally allowed to ring (at about 85 kHz) but is now damped (less than critical), the result being that only about 17% of the stored energy is actually dissipated in the discharge region (about 420 J at 12 kV).

The rotating-mirror camera used here was built in the department and uses an air turbine to rotate a martensitic stainless steel mirror approximately 50 mm square at speeds up to 1000 rev/sec. The maximum writing speed is 1 mm/μsec. Light reflected from a secondary mirror provides a timing pulse per revolution via a photosensitive semiconductor with suitable amplification, and this is displayed on an oscilloscope for speed setting; one of these pulses can be diverted to fire the experiment. Kodak Royal-X Pan 120 roll film is used giving eight exposures, no shutter other than a lens cap having been fitted to date, as the photography can be conveniently carried out in a darkened room and the experimental time is less than 0·001 sec, which is the minimum time required for the mirror to turn one revolution (only one face of the mirror is polished, the other is blackened). Axial slits of 0·4 mm width (in lengths from 18 to 36 cm) are mounted directly onto the shock tube and about 50 cm of the tube can be observed on one negative. The effective aperture is about f4 and the outside dimensions of the camera are 12 by 16 by 20 cm.

The spectroscope used is a Steinheil 3 glass prism unit of high dispersion. When taking time-resolved spectra the streak camera, with its lens removed, can be attached to the output arm and has sufficient aperture to accept, for example, a 500 Å band round the 4806 Å line of argon. There is some compromise at the moment between the desirable angled focal plane and the curved focal plane centred approximately round the mirror centre. The small bandwidth used does mean that the problem is not excessive.

III. Shock Structure

(*a*) *Streak Records*

The overall development of shock, driver, and discharge regions is most readily deduced from streak records that show the luminosity along the tube as a function of time. Two typical streak x–t diagrams are shown in Figures 3 and 4. The first points to be noticed on the streak photographs are multiple luminous fronts and the rapid attenuation of the leading luminous front. The multiple fronts were caused by a ringing discharge.

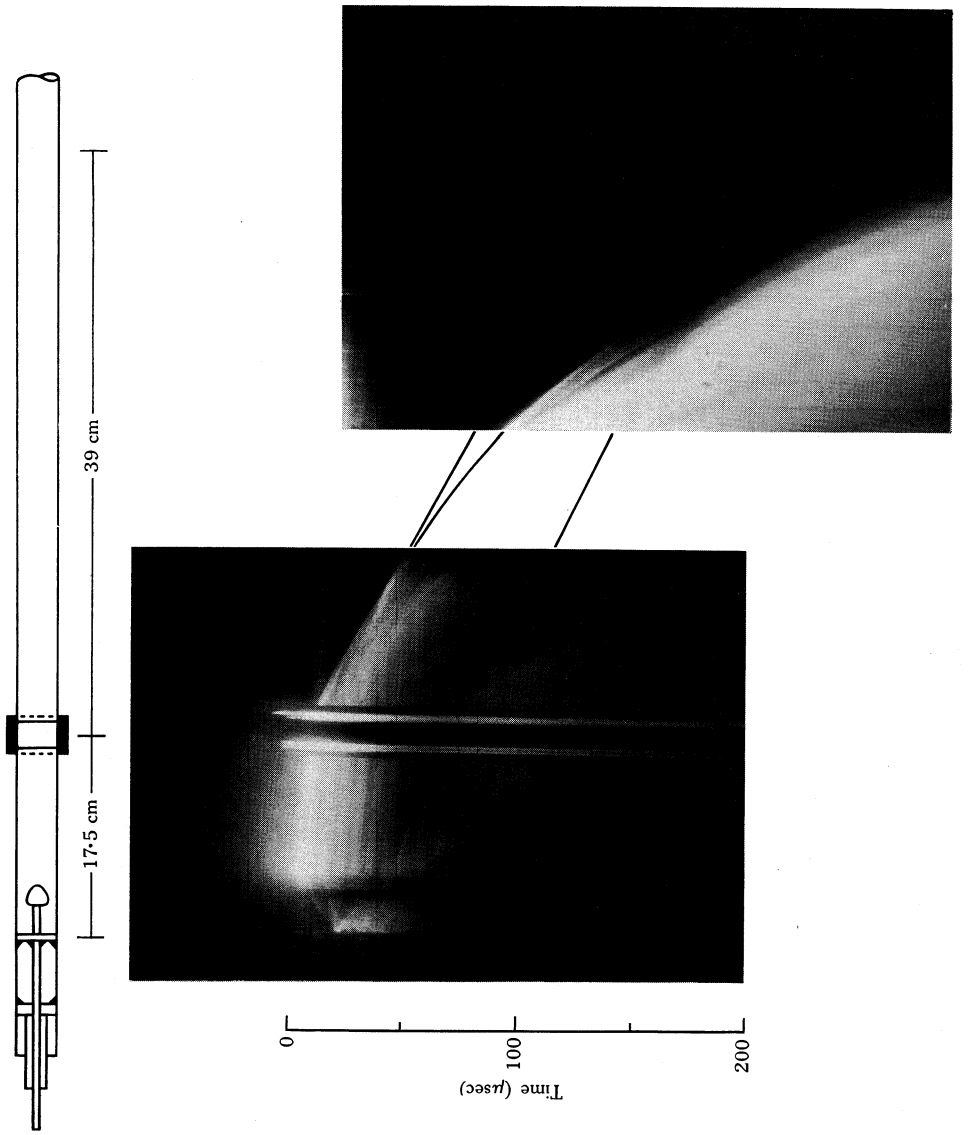

Fig. 3.—Composite x–t streak record of the total luminosity for a typical shock wave in air, with two different locations of the streak camera (downstream record taken at a greater aperture for increased detail).

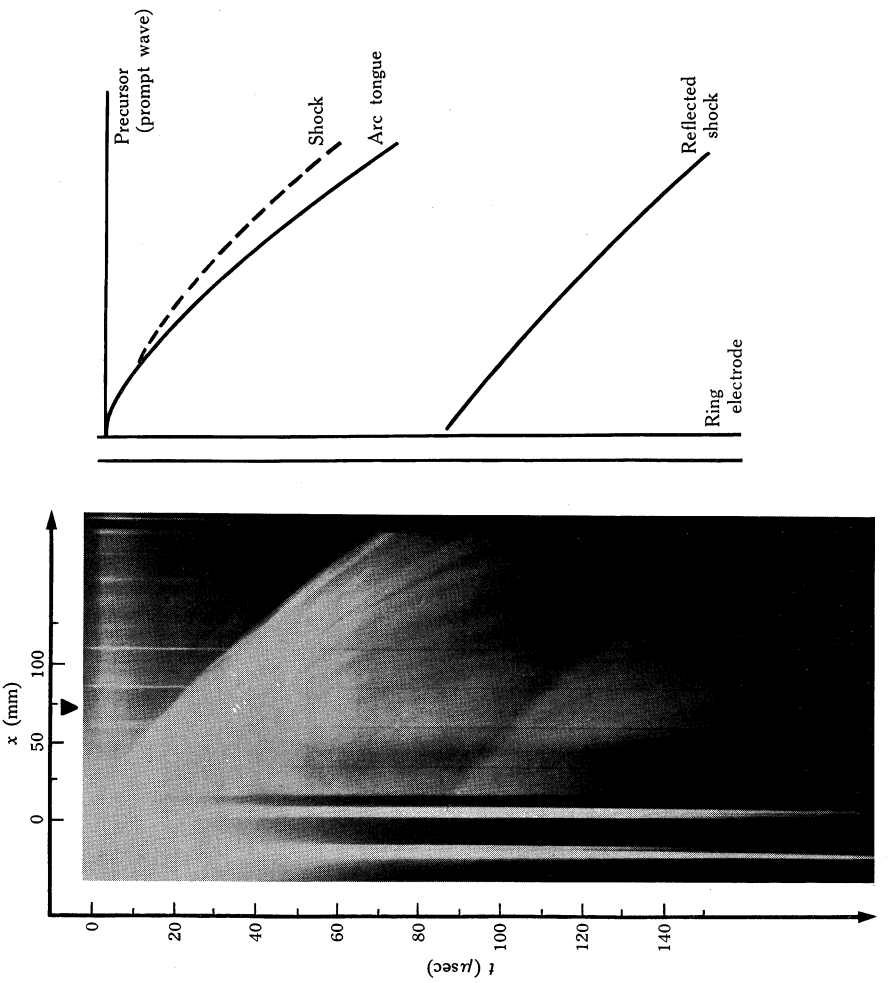

Fig. 4.—Single x–t streak record for argon at an initial pressure of 5 torr.

The streak photographs also show a second primary front that travels upstream until reflected from the back wall of the section of the tube containing the central electrode structure. The region between the tip of the central electrode and its backing plate is not heated by the discharge current—this leads to driver formation at both ends of the discharge region as can be seen in Figure 3. The driver moving to the left is reflected from the back wall and re-enters the hot region, catching up in due course with the driver that moved out to the right, as shown in Figures 3 and 4.

The streak record in Figure 3 was taken in air before damping resistors were incorporated. Figure 4 shows a record taken in argon at 5 torr with the capacitors (4 by 8·5 μF) charged to 12 kV and with a suitable damping resistor to reduce the discharge ringing to a single low energy restrike.

Both x–t records in Figures 3 and 4 present the same principal features. In the record for argon (Fig. 4) the luminosity is less for the shock heated region in front of the highly luminous driver. In fact the shock region cannot be seen on film once the tube is slightly coated with dust vaporized from the wall of the discharge section.

In both Figures 3 and 4, something resembling a precursor or "prompt wave" can be seen. Fowler (1963) claims a similar phenomenon to be an electron hydrodynamic wave travelling at about 10^8 cm/sec, and indeed other authors have detected electrons a short distance ahead of the shock, but our observations indicate that scattered light is the prime cause of the present luminous shaft. Streak photographs taken when the tube is scrupulously clean show a faint precursor, but after about 24 shots, when dust from erosion of the discharge chamber can be detected on the tube walls downstream from the driver, the film negative density due to the precursor is somewhat greater. The streak spectral work also supports the contention that this precursor is due to scattering of light from the primary discharge.

(*b*) *Nature of Shock Region*

The shock region indicated in the streak photographs is significantly smaller than would be inferred from conventional shock theory. Also the attenuation of the shock and driver fronts is quite severe. Thus a closer look at the nature of the propagating interfaces is warranted.

Static high speed photographs taken with an image converter camera (Abtronics Model 3) show a variety of fronts for the emergent arc tongue, many of which are steeply angled and very turbulent. As shown in Figure 5 planarity and homogeneity improve with pressure and progression down the tube. Very uneven fronts occur at low pressures ($\lesssim$ 1 torr) and these are associated with a particular form of filamentary breakdown in the initial discharge.

Because of the great disparity in luminosity between the shock-heated region and the arc tongue it has only been possible so far to photograph the arc tongue with the image converter camera, but some photographs taken well down the tube have shown evidence of a slightly luminous zone ahead of the arc tongue. Although the tongue fronts assume a greater planarity progressing down the tube it is hard to define the emergence and separation of a shock-front. An alternative explanation for the weakly luminous region ahead of the arc tongue could be that it represents a turbulent jet from the arc tongue itself. That this is not so can be deduced from

Figure 6, which is a streak photograph showing reflection of the low luminosity front from a ceramic end wall placed 20 cm downstream from the ring electrode. The gas used in this experiment was air at an initial pressure of 4 torr.

This x–t photograph shows in several ways that the low luminosity front behaves like a shock front and relevant data deduced from Figure 6 are shown below.

Incident shock speed	u_{si}	2810 m/sec
Incident shock temperature	t_{si}	3060°K
Reflected shock speed	u_{sr}	610 m/sec
Reflected shock temperature	t_{sr}	4800°K
Incident hot driver speed	u_{pi}	2320 m/sec
Reflected hot driver speed	u_{pr}	2385 m/sec
u_{si}/u_{pi}		1·2
u_{si}/u_{sr}		4·6
u_{pr}/u_{sr}		3·9

The low luminosity incident front velocity is greater than that of the arc tongue, making it unlikely that this region is due to a plasma filament thrown out by the arc tongue, as this would be expected to contract back towards the arc tongue due to cooling. The ratio of the low luminosity front velocity to the arc tongue velocity remains constant at 1·21. Also, the velocity upon reflection is seen to be considerably less than the incident velocity and the luminosity in the reflected zone increases. Increased luminosity must be due to either a particle temperature increase, an emitter density increase, or a combination of both.

The behaviour of the reflected wave in the electrically driven tube may be compared with a shock of the same incident Mach number and initial downstream pressure in air prepared with a mechanical shock tube and reflected from a rigid end wall (Glass 1958). For the mechanical shock tube, the ratio of incident to reflected shock speed is 4·9 and the same ratio for the electrical shock tube measured on Figure 6 is approximately 4·6. Consequently, we can identify the low luminosity region in front of the arc tongue as a shock-heated region.

In Figure 6 the reflected shock travels at constant velocity through the low luminosity zone until it approaches the arc tongue–shock interface where it accelerates rapidly and then proceeds again with almost constant but considerably higher velocity into the arc tongue.

The region in which acceleration occurs indicates that there is a temperature gradient or mixing region and not a sharp interface between the arc tongue and shock-heated regions. This temperature gradient is principally due to transitional turbulence at the arc tongue front, as indicated in the image converter photographs of Figure 5, and also possible radiative excitation of the shock region from the arc tongue. The fact that the reflected shock is accelerated implies also that it is moving into a hotter region (as expected) and the slight curvature in the trace as the reflected shock moves on indicates further small acceleration towards the discharge chamber.

It is important to compare the results of these optical investigations with the earlier studies made with probes or electrodes inserted into the expansion region of the shock tube (George and Messerle 1962; George, Heffernan, and Messerle 1964). Originally these were carried out fairly close to the ring electrode and it

was often difficult to distinguish a shock-heated region from the arc tongue, although applied voltage tests (e.g. Fig. 8 of George, Heffernan, and Messerle 1964) were able to show the presence of pre-ionized gas ahead of the driver. The shock nature of the flow was deduced from speed measurements, which showed a difference of 20% between the shock front arrival speed and the mass flow rate calculated from induced voltages between the probes in air. This corresponded to streak record data taken at a later date.

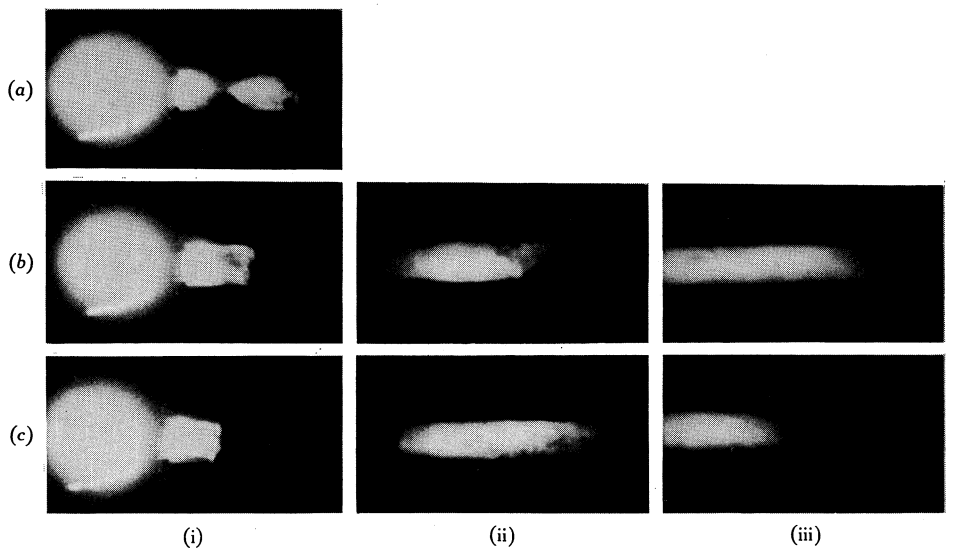

Fig. 5.—Image converter photographs of the arc tongue in argon at different pressures under 14 kV and 17 μF conditions taken at the times indicated:

(*a*) 1 torr initial pressure, (i) 20 μsec delay;

(*b*) 5 torr initial pressure, (i) 20 μsec, (ii) 45 μsec, (iii) 190 μsec delay;

(*c*) 10 torr initial pressure, (i) 20 μsec, (ii) 60 μsec, (iii) 220 μsec delay.

When the discharge energy is increased and when probe measurements are carried out further downstream clear evidence is obtained of a colder, less-conducting region ahead of the driver, as seen in Figure 7. These records show the voltages induced between two probes when a transverse magnetic field is applied at a probe station 15 cm from the ring electrode. The voltages are seen to rise to their full open-circuit value (10 V) in about 1 μsec and remain at this value as both the shock-heated region and the arc tongue pass the probe station. However, the difference between the two regions can be clearly shown when the probes are loaded by an external resistance R_t. Under these conditions the terminal voltage drops to a value determined by the ratio of the internal resistance between the probes to the external resistance and thus becomes a measure of the gas conductivity. In Figure 7 two such isolated pairs of probes are being used at the same time, one of which is left open-circuited to monitor the true open-circuit voltage on each occasion.

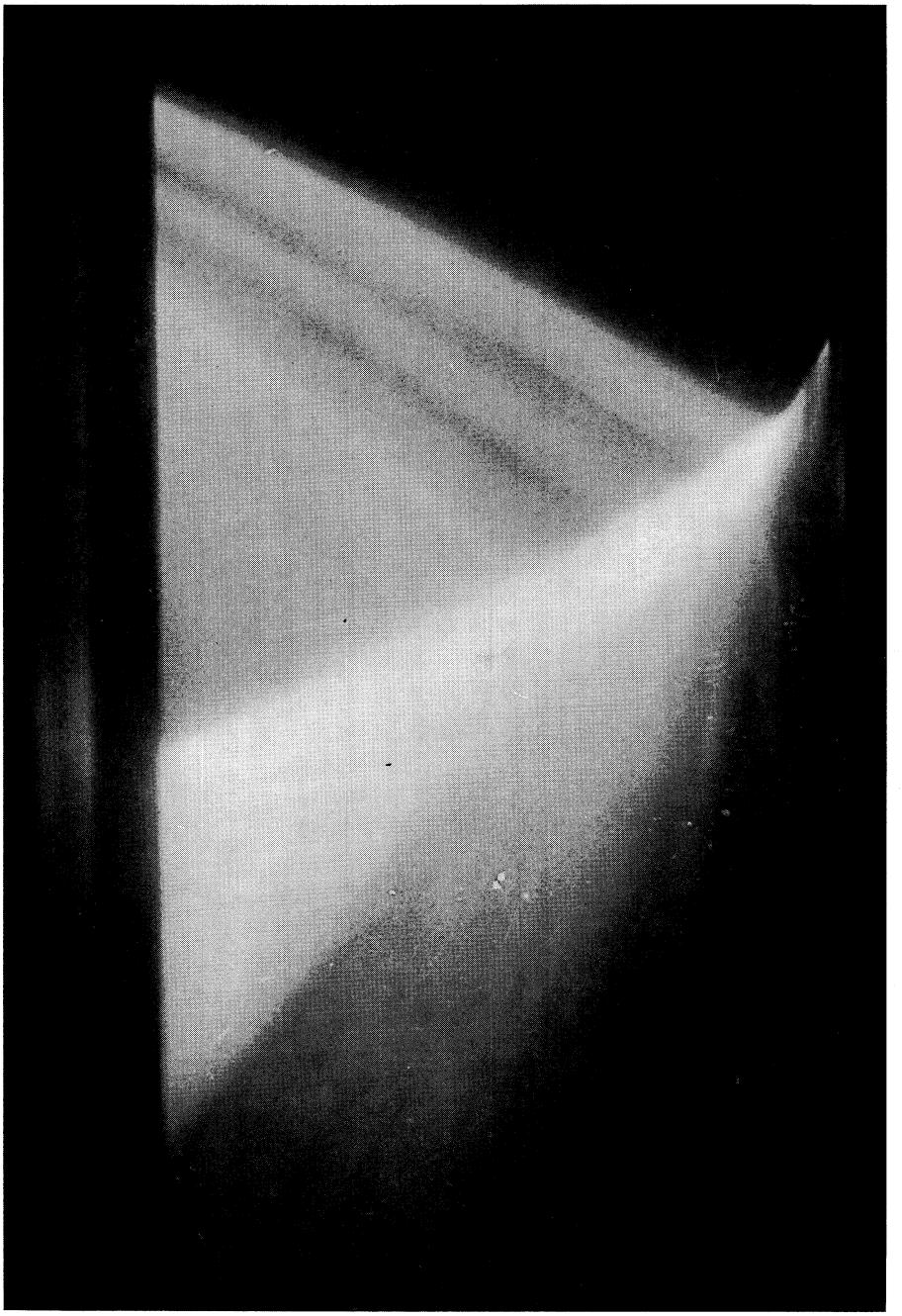

Fig. 6.—Single x–t streak record of a shock in air at 5 torr initial pressure that is reflected from a ceramic end wall 20 cm from the ring electrode.

In Figure 7(*a*) both pairs of probes are on open circuit and the wave shapes are identical. However, with an external resistance of 33 kΩ (Fig. 7(*b*)) the voltage in the shock-heated region is already halved whilst the following gas shows no effect of loading, i.e. has a very much higher electrical conductivity. An external resistance of 330 Ω (Fig. 7(*d*)) has completely short-circuited the initial region and is only just beginning to "load" the gas in the arc tongue region. For this latter region a resistance of as low as 10 Ω (Fig. 7(*f*)) is required to short-circuit the terminals.

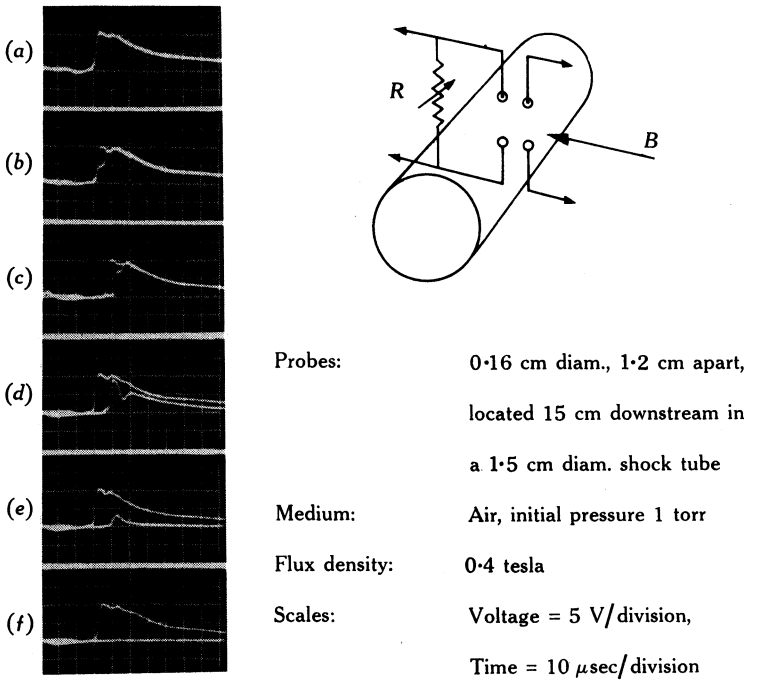

Fig. 7.—Double probe induced voltage records (one pair recording the open circuit voltage, the other pair being loaded by a variable resistance) showing (in (*b*) and (*c*)) the presence of a colder shock heated gas layer ahead of the arc tongue or driver. The load resistances are:

(*a*) open circuit, (*b*) 33 000 Ω, (*c*) 3300 Ω,
(*d*) 300 Ω, (*e*) 33 Ω, (*f*) 10 Ω.

From these and similar probe results, various conclusions can be drawn regarding the nature of the shock propagation. Since the particles in the low conductivity region at the front of the expansion are able to induce the same magnitude of voltage as those in the arc tongue, the particle velocities in both regions are identical, as required for normal shock propagation. (Such a conclusion could not have been drawn from earlier tests with applied voltages since the low conductivity region could have been caused by different forms of pre-ionization.) Also, the much smaller electrical conductivity of the gas ahead of the arc is as expected for a lower temperature shock-heated region. However, close examination of the probe results reveals the presence of turbulence in the gas sample which has not been noted previously.

Thus Figures 7(*d*) and 7(*e*) show the maxima of electrical conductivity occurring at slightly different distances behind the shock front, and in Figure 7(*d*) the presence of a second maximum can be seen. Similarly the shock-heated region has a variable conductivity structure, the first half being of uniform conductivity (corresponding to an internal resistance of 33 kΩ, Fig. 7(*b*)), followed by a higher conductivity region (Figs. 7(*c*) and 7(*d*)) due to turbulence or mixing at the driver–shock interface.

Thus it has been clearly established from both the electrical and optical measurements that the electrically driven shock tube is able to produce a shock-heated gas region of a conventional type ahead of the expanding driver gas.

IV. Spectroscopic Measurements

(*a*) *Spectral Techniques*

Spectroscopic techniques have been pursued because they offer a method of probing the plasma without the contaminating effect of insertion devices, the work to date attempting to determine time-resolved electron densities and gas temperatures in the various regions and to confirm the plasma purity.

Temperature determination by the relative line intensity method requires a basic assumption of local thermodynamic equilibrium which is not necessarily true in the experimental situation, and which must therefore be shown to be true by achieving the same temperature over many different line pairs or constructing an Arrhenius plot. The electron density, however, may be determined by a method largely independent of equilibrium considerations, namely Stark broadening, using in particular the 4861 Å line of hydrogen (Hβ) for which much theoretical and experimental work has already been done by Baranger (1959), Griem, Kolb, and Shen (1959), and Griem (1964). The agreement between experimentally and theoretically determined profiles for this particular line is better than $\pm 3{\cdot}5\%$ (Hill and Gerardo 1967). The Hβ contour may be described in terms of its halfwidth; Huddlestone and Leonard (1965), for example, give a graph for electron density based on the Hβ intensity halfwidth (p. 309).

To use this technique with a pure gas such as argon, it is necessary to introduce a small amount of hydrogen for diagnostic purposes. In the present experiments the amount introduced was about 1% or less.

Photographic techniques are being used with the spectroscope because this provides a lot of information in a single shot; there are, however, certain difficulties inherent in the nonlinearity of the photographic emulsion which point up some advantages of the photomultiplier.

Static spectrograms were taken to provide information on the impurities at different parts of the experiment, all the lines on the spectrograms have been measured from the 4916 Å mercury reference line, which is the plate centre, the approximate value or tentative identification being read off a very large dispersion curve. The lines were then finally identified from the M.I.T. wavelength tables (Harrison 1939). It is worth noting that the greatest difference over the whole plate was 0·9 Å. This gives a high degree of confidence in the line identification here although parts per million impurities in the EG3 graphite ring electrode could furnish Ca I, Ca II, Ba I, or Ba II lines, which are very close to some of the argon lines identified in

the 500 Å band about the Hβ line in the streak spectra. The beacon lines or "raies ultimes" of these elements do not appear on the static spectrograms however; consequently these impurities may be discounted.

A static spectrogram cannot be used in this transient work to obtain results from intensity ratios as it is normally exposed for the whole duration of the hot driver passage and integrates the intensities over this period. This objection can be overcome by connecting the streak camera with its lens removed to the output of the spectroscope, the entrance slit height of which is adjusted to give an acceptable integration time (short compared to experimental time) at the film plane. In this way line intensity is displayed against time, and by measuring the intensity across the spectrum at successive positions down the line of sweep, a series of time-resolved results may be obtained for each shot. The time variations of the width of the Hβ line as well as of the line intensities are shown in the streak spectrogram in Figure 8.

(*b*) *Comments on the Use of Photographic Techniques*

It is worth mentioning some of the difficulties involved in using photographic techniques for quantitative results.

A basic assumption made is that of reciprocity, which broadly states that for identical development conditions a given exposure will always produce the same negative density, though in one case the intensity is high and the exposure time very short, and in another the intensity is low and the exposure time very long. The reciprocity law may be written

$$E = \int I \, \mathrm{d}t,$$

where E is the exposure, I the intensity, and t the exposure time. This law is true for modern films for a time scale from 100 to 0·0001 sec but no single film has this latitude and different emulsions are required, ranging from fine grain at the slow end to coarse grain for high speed film. Beyond the limits for a particular film there is failure of the reciprocity law, and a suitable multiplying factor must be obtained from the manufacturer's reciprocity failure data curves.

A certain amount of energy is necessary to allow the image sites to become established either on or within the crystals making up the emulsion. These sites may or may not be developable under normal conditions, and so either developable or subdevelopable latent images may be formed (Mees 1954). If the light level is such as to make a subdevelopable latent image likely, techniques such as pre-exciting the film by exposing it to faint light before exposure or harsh developing after exposure, using bleaching developer to expose sites within the grain, may be employed in order to make the image developable.

In the present streak photographs the energy falling on the film in the far wings of the broadened Hβ line could well be close to the subdevelopable image condition thus affecting the shape of the line profile. The continuum under the Hβ line also contributes to the energizing of the film, reducing the profile error but causing an uncertainty when trying to determine the continuum contribution by joining the continuum on either side of the line profile. This effect can in turn be reduced by film pre-exposure as already mentioned. The centre portion of the line by virtue

of its strong exposure is little affected and the line intensity halfwidth is readily determined, knowing the characteristic curve for the film. Since electron density is expressible in terms of the halfwidth the entire profile is not required. It would be necessary to use caution if the experimental profile were to be matched to the theoretical profile because of the possible reduction in the far wings.

(*c*) *Time-resolved Hβ Line*

In Figure 8(*b*) are a series of intensity scans taken at various time intervals through the streak spectrum. The broadening and splitting of the Hβ line is very obvious in the photograph (Fig. 8(*a*)); it splits virtually symmetrically, and can be clearly seen in the tracings to have a slightly higher peak towards the blue end, which agrees well with theory. The film used here was Kodak Royal-X Pan and is one of the fastest roll films commercially available, being capable of force developing to 5000 ASA. Being fast it is also large grained and hence noisy on the Zeiss Jena microdensitometer which is used to scan the negative.

Considering the streak spectra we can identify initially, when the discharge is fired, an A II spectrum with no Hβ and no Si II impurity. This is the radiation emitted from the so-called precursor. Its commencement time is almost the same as the commencement of breakdown, and its duration agrees with photomultiplier timing of primary discharge luminosity. Lack of impurity silicon spectra agrees with the hypothesis that couples precursor radiation to the primary discharge peak, as plasma contact with the wall would tend to be more effective after this time. The non-appearance of the Hβ line in the precursor radiation is due to the level of ionization being so high in the discharge core that the number density of Hβ emitters is greatly reduced.

Calculations based on the velocity of the shock front (Mach 11·5) for the shock shown in Figure 8 place its temperature at around 10 500°K, and at this temperature argon is only slightly ionized and will radiate predominantly A I spectra. However, there is no indication of any A I lines preceding the arc tongue, so it is reasonable to assume that the radiation intensity from the shock region is relatively low, as expected from the *x–t* streak photographs.

The Hβ line can be seen to broaden twice during the passage of the arc tongue. This is due to the fact that the discharge is still somewhat underdamped (see Fig. 10 for energy input) and a front due to the secondary discharge is passing through the hot primary tongue.

In determining the halfwidth and hence the electron density we have allowed for the considerable continuum under the line by carrying the average continuum at the sides through and subtracting this. The effect of this sort of correction can be reduced by adding a controlled amount of hydrogen as mentioned, giving considerably more emitters, instead of relying on the variable amounts of water vapour impurity in the argon. Allowance must also be made for the film characteristics.

Figure 9 shows the plot of electron density as determined by the microdensitometer scans of the swept spectra on the same time axis as the *x–t* streak. The electron density peaks can be seen to correspond to stria in the arc tongue, the first peak being the primary tongue and the second the secondary tongue due to the underdamping.

Fig. 8.—Streak spectra (*a*) for an argon shock at an initial pressure of 5 torr, and intensity scans (*b*) taken at appropriate intervals across the plate.

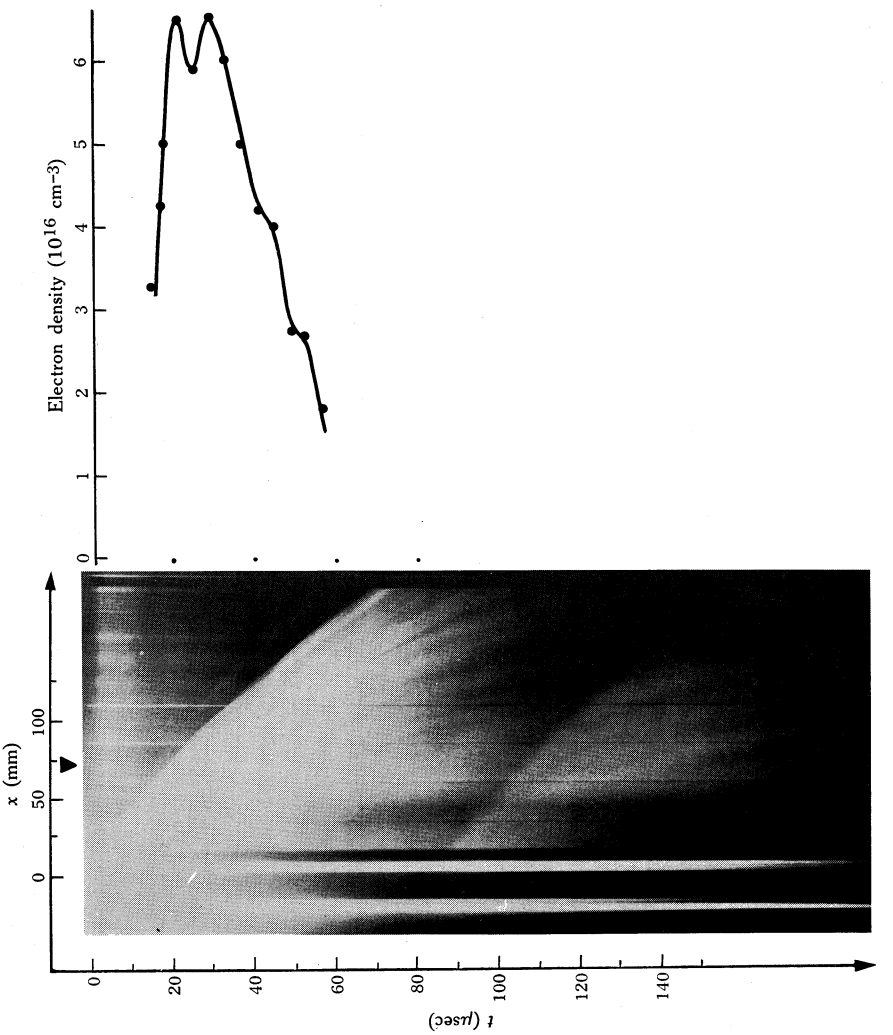

Fig. 9.—Electron density as a function of time at a point 70 mm downstream from the ring electrode for an argon shock similar to that shown in Figure 4.

V. Temperature Estimations

(a) *Discharge Region*

An approximate initial temperature in the discharge region can be determined by estimating the increase in internal energy in the region due to the capacitive discharge and then using tables of thermodynamic data (in this case prepared by Drellishak, Knopp, and Cambel 1963) for the particular gas. In using these tables we assume that equilibrium conditions are established before the driver develops. While in the first few microseconds the electron and heavy particle temperatures are definitely not the same, the plasma does not emerge from the ring electrode until almost the entire power pulse has been delivered, by which time the two temperatures are similar.

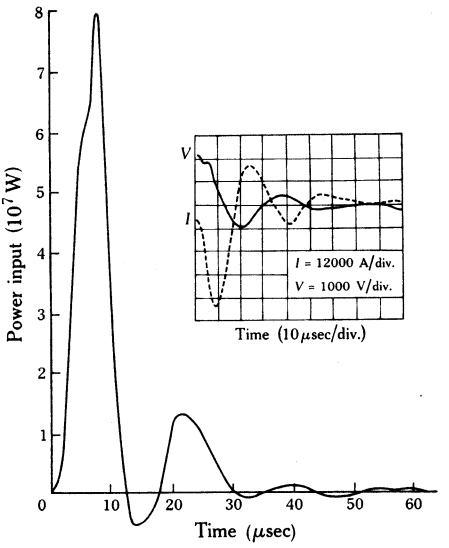

Fig. 10.—Power input as a function of time obtained from the discharge current and voltage waveshapes shown in the inset.

In determining the internal energy the electrical energy input is found from the current and voltage characteristics of the discharge. The voltage is measured using a Tektronix type P6015 high voltage probe and type 555 oscilloscope, and the current is measured using a re-entrant non-inductive shunt (Grimwood 1965). Two traces appropriate for the shock shown in Figure 9 are given in the insert of Figure 10.

The initial conditions for this shock were: initial pressure, 5 torr argon; total capacitance, 34 μF; capacitor voltage, 12 kV; stored energy ($\frac{1}{2}CV^2$), 2450 J. Integration of the curve in Figure 10 for the first power cycle shows that the energy into the discharge is 420 J, which corresponds to an efficiency of 17%.

The internal energy increase was calculated as $5{\cdot}2\times10^4$ cal/g, by considering a static volume of the gas slightly greater than that defined between the electrodes. The length of this volume can be determined from a streak photograph, such as Figure 3, by extrapolating the downstream and upstream shock fronts back to their origins, which are respectively the centre of the ring electrode and within 5 mm of the central electrode tip on the upstream side.

Since expansion starts very late in the power pulse the heating can be considered to be at constant mass density. With this assumption and the above value of internal energy, extrapolation of data given by Drellishak, Knopp, and Cambel (1963) yields a temperature of approximately 42 000°K. At this temperature the pressure in the discharge region rises to 2·8 atm, giving a pressure ratio of 426.

(*b*) *Shock-heated Region*

It has already been shown that standard shock equations can be applied to the shock-heated regions in the present experiment. For the shock in Figure 9, measurements were taken from the streak photograph 70 mm downstream from the ring electrode, giving a speed of 3700 m/sec, or Mach 11·5. From calculations using data allowing for ionization, the temperature corresponding to this speed in argon was found to be 10 500°K and the pressure ratio approximately 170.

(*c*) *Hot Driver* (*Arc Tongue*) *Region*

Streak spectrograms of the arc tongue show a strongly broadened Hβ line and consequently the electron density can be determined. Although Stark broadening theory does not require a Boltzmann distribution, it is most probable that such a distribution exists here, following the arguments for the discharge region. In this case if the pressure is known the temperature may also be determined. A time-resolved plot of electron density in the arc tongue is given in Figure 9, the peak density at the front being approximately $6{\cdot}6\text{–}7 \times 10^{16}$ electrons/cm.^{3}

Because of continuity considerations across the boundary between the shock-heated region and the hot driver, the pressure at the hot driver interface will be the same as in the shock, i.e. 1·1 atm. For these values the tables by Drellishak, Knopp, and Cambel (1963) yield a temperature of 12 100°K.

Values for the different regions for the shock in argon shown in Figure 9 may be summarized as follows:

	Pressure (atm)	Temperature (°K)	Velocity (m/sec)	Mass Density (10^{-5} g/cm^3)
Discharge region	2·8	42 000	—	1·18
Arc tongue region	1·1	12 100	3200	3·7
Shock region	1·1	10 500	3700	5·0

VI. Conclusions

The experimental results tie in with the assumption that the electrothermal shock tube performs like a mechanical shock tube with a hot driver. One could still suspect some electromagnetic drive effects due to trapped circulating currents in the hot arc tongue, but extensive tests using magnetic probes did not show up any currents after the discharge had been extinguished.

The interface between driver and shock has been observed to be quite turbulent, thus preventing the early development of a clearly definable shock region. The detection of the shock region is made difficult because of the much higher temperature in the driver region, but a shock region can be seen to develop after the arc tongue or hot driver has moved some distance downstream.

The main reason for the turbulence at the driver–shock interface appears to be the fact that the density in the driver is lower than that in the shock region. As shown in the data above, the temperature in the driver is higher than that in the shock and, assuming pressure equality across the interface, the density in the driver must be less. Consequently we have a low density driver pushing a shock region that is at a higher density, and this is a condition for a Taylor-type interface instability.

The density in the driver head, although below that of the shock region, is actually much higher than expected if the driver was simply due to an expansion of the gas in the high pressure discharge region. If it was due to expansion only it should be less than the value of $1{\cdot}18\times10^{-5}$ g/cm^3 quoted above for the density of the discharge region. This higher density is really to be expected when allowance is made for the interface instability, which results in a mixing of shock and driver gas at the interface. As a consequence of this mixing the head of the driver is more dense than the rest of the driver.

The instability at the driver–shock interface seems to result in poor shock structure and high attenuation in electrically driven shock tubes, and this probably accounts for the fact that no shock regions have been observed in front of ultra high velocity "ionizing fronts" in electromagnetic shock tubes.

VII. Acknowledgments

The authors would like to acknowledge the financial assistance provided by the Electrical Research Board and the Australian Institute of Nuclear Science and Engineering.

VIII. References

Baranger, M. (1959).—*Phys. Rev.* **111**, 494.

Cloupeau, M. (1963).—*Phys. Fluids* **6**, 679.

Drellishak, K. S., Knopp, C. F., and Cambel, A. B. (1963).—U.S. Air Force Systems Command Technical Documentary Rep. No. AEDC-TDR-63-146.

Fowler, R. G. (1963).—U.S. Office of Naval Research, Contract No. Nonr. -982 (02).

Fowler, R. G. (1966).—*Rev. scient. Instrum.* **37**, 545.

George, D. W., Heffernan, L. P., and Messerle, H. K. (1964).—*Electl mech. Engng Trans. Instn Engrs Aust.* E.M. **6**, 29.

George, D. W., and Messerle, H. K. (1962).—*J. Fluid Mech.* **13**, 465.

Glass, I. I. (1958).—Shock Tubes, Part I; Theory and performance of simple shock tubes. University of Toronto Institute of Aerophysics Review No. 12.

Griem, H. R. (1964).—"Plasma Spectroscopy." (McGraw-Hill: New York.)

Griem, H. R., Kolb, A. C., and Shen, K. Y. (1959).—*Phys. Rev.* **116**, 4.

Grimwood, P. (1965).—M.Eng.Sc. Thesis, University of Sydney.

Harrison, G. R. (1939).—"Wavelength Tables." (Wiley: New York.)

Hill, R. A., and Gerardo, J. B. (1967).—*Phys. Rev.* **162**, 45.

Huddlestone, R. H., and Leonard, S. L. (1965).—"Plasma Diagnostic Techniques." (Academic Press: New York.)

Kolb, A. C. (1959).—Proc. 4th Int. Conf. on Ionisation Phenomena in Gases. Vol. IVC, p. 1021.

Mees, C. E. K. (1954).—"Theory of the Photographic Process." (Macmillan: New York.)

Messerle, H. K., and George, D. W. (1963).—*Phys. Fluids* **6**, 1777.

Sakuntala, M., Von Engel, A., and Fowler, R. G. (1960).—*Phys. Rev.* **118**, 1459.